



HAL
open science

Time-evolution of the structure of organoclay/polypropylene nanocomposites and application of the time/temperature superposition principle

Riadh Zouari, Trystan Domenech, Bruno Vergnes, Edith Peuvrel-Disdier

► **To cite this version:**

Riadh Zouari, Trystan Domenech, Bruno Vergnes, Edith Peuvrel-Disdier. Time-evolution of the structure of organoclay/polypropylene nanocomposites and application of the time/temperature superposition principle. *Journal of Rheology*, 2012, 56 (4), pp.725-734. 10.1122/1.4708602 . hal-00700469

HAL Id: hal-00700469

<https://minesparis-psl.hal.science/hal-00700469>

Submitted on 13 Apr 2017

HAL is a multi-disciplinary open access archive for the deposit and dissemination of scientific research documents, whether they are published or not. The documents may come from teaching and research institutions in France or abroad, or from public or private research centers.

L'archive ouverte pluridisciplinaire **HAL**, est destinée au dépôt et à la diffusion de documents scientifiques de niveau recherche, publiés ou non, émanant des établissements d'enseignement et de recherche français ou étrangers, des laboratoires publics ou privés.

**TIME-EVOLUTION OF THE STRUCTURE OF
ORGANOCLAY/ POLYPROPYLENE NANOCOMPOSITES
AND APPLICATION OF THE
TIME/TEMPERATURE SUPERPOSITION PRINCIPLE**

R. Zouari, T. Domenech, B. Vergnes, E. Peuvrel-Disdier

MINES ParisTech, Centre de Mise en Forme des Matériaux (CEMEF),

UMR CNRS 7635, BP 207, 06904 Sophia-Antipolis Cedex (France)

Synopsis

We investigated the rheological properties of nanocomposites composed of polypropylene, organoclay and maleic anhydride grafted polypropylene in small amplitude oscillatory shear. Samples were prepared in two steps: a masterbatch was first obtained by melt extrusion and then diluted into polypropylene using an internal mixer. Three formulations were investigated. The measurement of the storage and loss moduli evolution with time showed that these materials were not stable: the nanostructure obtained after steady shear continuously changed with time, due to the disorientation of the clay platelets and the build-up of a 3D network. The kinetics of the structure built-up (followed via the melt yield stress) showed a two-step process. This feature was found to be valid whatever the nanocomposite formulation. Such evolution of the structure is generally assumed to violate the time-temperature superposition principle. We demonstrate in this paper that the time-temperature equivalence always exists if the same nanostructure is probed. This was achieved by using different annealing times for different temperatures or annealing the samples at the highest temperature before measuring at lower values. The time-temperature equivalence evidences that the temperature does not induce any chemical change within the material whose properties remain governed by the same physical phenomena.

I. INTRODUCTION

Since the pioneering work of Toyota on polyamide nanocomposites, nanocomposites based on organically modified layered silicates (organoclays) have received a considerable attention for some years [Alexandre and Dubois (2000); Palvidou and Papaspyrides (2008); Paul and Robeson (2008)]. Nanocomposites based on organoclays exhibit for very low clay loadings enhanced properties like mechanical properties [Krishnamoorti *et al.* (1996); Ren *et al.* (2000)], flame retardancy and increased thermal stability [Gilman (1999)], as well as lower permeability to gases [Messersmith and Giannelis (1995); Xu *et al.* (2001)] when compared to pure polymers. One of the key scientific and technical challenges in these materials is the control of the particulate structure to be reached in order to achieve the desired properties. The common idea is that a stable fully dispersed state is necessary to obtain enhanced properties.

Due to its characteristics, there is a large interest in polypropylene based nanocomposites. However, even though organomodified nanoclays are used, the dispersion in a non-polar matrix is difficult and necessitates to use a compatibilizer (polypropylene grafted with maleic anhydride (PP-g-MA) in most studies) [Solomon *et al.* (2001); Lertwimolnun and Vergnes (2005); Nazockdast *et al.* (2008)].

The dispersion state and the nanocomposite structure can vary from simple intercalation of the silicate layers by the polymer chains to total exfoliation (individual layers). Generally, a mixed structure with intercalated tactoids and partially exfoliated platelets is observed, possibly forming a 3D network. The nanoclay dispersion state and associated nanocomposite structure can be characterized via complementary techniques, like X-ray scattering to evaluate the interlayer spacing. It can also be visualized by transmission electronic microscopy (TEM) even if this technique remains very local and not really adapted to observe a 3D structure. On another hand, rheometry constitutes a powerful technique to detect and characterize a percolated system as proven in the literature [Krishnamoorti and Giannelis (1997), Loiseau and Tassin (2005), Vermant *et al.* (2007); Cassagnau (2008); Mobuchon *et al.* (2009); Elasmı *et al.* (2010)]. In particular, linear viscoelastic measurements at low frequencies are sensitive to the interactions between particles inside the polymer and their evolution within the system. In fact, a percolated network shows a solid-like behavior with a low frequency domain characterized by the presence of an elastic plateau and an increase of the complex viscosity. Lertwimolnun and Vergnes (2005) were the first to propose to use the Carreau-Yasuda law with a yield stress to represent the viscosity variation at low frequency. They have shown that

the yield stress value is correlated to the degree of exfoliation of the nanocomposite. Vergnes (2011) has recently shown the interest in using this parameter to describe the nanocomposite structure.

Although nanocomposite materials received a lot of interest in the last years, the exact nature of the nanocomposite structure is still an open question. Depending on the nanoclay state (from intercalated to fully exfoliated), the rheological behavior lies between a liquid-like and a solid-like one. The solid-like behavior is associated to the presence of a 3D structure where the nanoclays form a more or less soft network. This network can be seen as a nanoclay network formed by platelets and tactoids, as attractive forces between the clay platelets exist and play a role in the network properties. Moreover, it has been shown that this nanostructure can change with time or temperature, which renders the comprehension of the system more and more complicated. For sake of simplicity, the nanocomposite structure will be referred to nanoclay network or 3D network in the following.

Most of the studies dedicated to the investigation of the linear viscoelastic properties of nanocomposites assume that the sample structure does not change during small amplitude oscillatory shear experiments. This stability generally comes from chemical or thermal treatments of the samples [Krishnamoorti and Giannelis (1997); Nazockdast *et al.* (2008)]. Under these conditions, no remarkable structural changes occur within the material, at least in the experiment time scale, for different temperatures. Thereby, some investigations showed that the phenomenological time-temperature superposition principle (TTS) applies and a mastercurve could be obtained to describe the rheological behavior of the nanostructured material on a broader frequency range than that allowed by the rheometer [Solomon *et al.* (2001)]. To the best of our knowledge, studies dealing with time evolutive nanostructured materials did not mention any time-temperature equivalence and the authors investigated rheological features associated to the sample at a fixed temperature with well defined protocols [Reichert *et al.* (2001); Ren *et al.* (2003); Mobuchon *et al.* (2007, 2009)]. However, some authors found some failures by applying TTS, principally in the low frequency range [Zhao *et al.* (2005); Treece and Oberhauser (2007a,b)]. Reichert *et al.* (2001), Wagener and Reisinger (2003) and Drozdov *et al.* (2010) mentioned that the structure change within the nanocomposite leads to a violation of the TTS principle. Reichert *et al.* (2001) have checked the validity of the TTS principle applied to extruded and injection molded PP nanocomposite samples with an unstable morphology and concluded that the TTS principle does not hold

unless a thermal treatment (ageing) is applied to the samples at the highest tested temperature during 200 min, to ensure that they are in a thermodynamically stable state.

The aim of the present work is to report about the development of the nanostructure during an annealing process and the corresponding applicability of TTS principle. The conditions related to a successful application of the TTS principle will be presented as well as information about the mechanisms leading to the formation of a 3D network within the polymer matrix.

II. EXPERIMENTAL PART

A. Materials

The organoclay was provided by Laviosa Chimica Mineraria (Italy). The Dellite[®] 67G organomodified montmorillonite (OMMT) was chosen for its compatibility with polyolefins. Its surfactant is a dimethyl dihydrogenated tallow alkyl ammonium and its cation exchange capacity (CEC) is 115 meq/100 g. Scanning Electron Microscopy (SEM) observations of the Dellite[®] 67G at different magnifications showed agglomerates with a diameter lying between 20 and 40 μm . It gives an idea of how important is the role of the dispersion process to reach a nanoscale structure, starting with 40 μm agglomerates to end up with single platelets of 1 nm in thickness and 500 nm in lateral dimensions.

The selected matrix was an injection grade isotactic polypropylene (PP) produced by LyondellBasell under reference Moplen HP400R ($M_w = 233\,300$ g/mol).

A polypropylene grafted with maleic anhydride (PP-g-MA) was used as a compatibilizer. The selected PP-g-MA is produced by Eastman as Epolene G-3015. Its maleic anhydride content is 3% in weight.

B. Samples preparation

The nanocomposites were obtained by dilution into the polypropylene matrix of masterbatches containing the organoclay. Two masterbatches were prepared by twin screw extrusion on a laboratory extruder Brabender PL2000, in the same processing conditions: processing temperature 200°C, flow rate 5 kg/h, screw speed 200 rpm. The first one contained only PP-g-MA (80 wt%) and OMMT (20 wt%), the second contained 20 wt% of OMMT, 40 wt% of PP-g-MA and 40 wt% of PP. The ratio PP-g-MA/OMMT was thus 4 and 2,

respectively. These masterbatches were then diluted into the PP matrix using an internal mixer (Haake Rheomix 600) at 180°C, with a rotor speed of 100 rpm during 10 min. The final compositions of the three nanocomposites investigated in this study are indicated in Table 1. Samples A and B have the same OMMT content (5 wt%) and differ by the PP-g-MA/OMMT ratio and thus the level of exfoliation. Samples B and C have got the same PP-g-MA/OMMT ratio, but different amounts of OMMT (5 and 7 wt%, respectively). In all cases, OMMT content is much higher than the percolation threshold, measured at 3 wt% for samples B and C. This threshold was not measured for sample A. It is probably slightly higher, as the exfoliation is expected to be lower, but smaller than 5%. All the samples extracted from the internal mixer were then compression moulded (at 180°C and 25 MPa for 10 min, followed by cooling down to room temperature) in order to obtain disks with controlled thickness ($e = 1$ mm) and diameter ($D = 25$ mm)

Table 1. Composition of the nanocomposites

| Sample | PP (wt%) | PP-g-MA (wt%) | OMMT (wt%) | PP-g-MA/OMMT |
|--------|----------|---------------|------------|--------------|
| A | 85 | 10 | 5 | 2 |
| B | 75 | 20 | 5 | 4 |
| C | 65 | 28 | 7 | 4 |

C. X-ray diffraction measurements

Wide Angle X-ray Diffraction (WAXD) experiments were conducted on the compressed samples with a Philips X'pert Pro diffractometer with Cu K α radiation of wavelength 1.54 Å. The accelerating voltage was 40 kV. Diffraction spectra were obtained over 2θ range lying between 2 and 10° and the interlayer spacing d_{001} was calculated using the Bragg's equation: $\lambda = 2d \sin \theta$, where λ is the wavelength.

D. Morphological characterization

Microscopic scale observations of the nanocomposites structure were achieved using a Scanning Electron Microscope (SEM) Philips XL30 ESEM, equipped with a LaB₆ cathode, under an acceleration voltage of 15 kV. Pictures have been acquired using a back scattered

electron detector to allow high phase contrast between matrix and OMMT. Prior to observations, samples were successively polished to access core-structure on a flat surface (surface roughness less than 1 μm) and metallized (Au/Pd coating of 100 \AA) to enhance samples electronic conductivity.

Observations at the nanoscopic scale were carried out with a Transmission Electron Microscope (TEM) Philips CM12, equipped with a LaB₆ cathode, under an acceleration voltage of 120 kV. Ultrathin sections of the samples were prepared at -100°C from the cross section of an injection moulded tensile bar (in the central zone), using an Leica Ultracut ultracryomicrotome mounted with Diatome Cryotrim and Cryo diamond knives. The sections, with nominal thickness of 50 nm, were transferred to 200 mesh copper grids and dried at room temperature using filter paper.

E. Rheological characterization

The rheological measurements were conducted on an ARES (TA Instruments) strain-controlled rotational rheometer. Measurements were performed at 180°C, 200°C and 220°C, using either a parallel plate or a cone and plate geometry, with a cone angle of 0.0401 rad. Plate diameter was 25 mm and the gap for the parallel plate geometry was 0.5 mm. In order to minimize the deformation history and all phenomena associated to the preparation and the loading of the sample in the gap, a permanent shear was applied to the sample, prior to any measurement. It consisted in shearing the material at 1 s^{-1} during 155 s to destroy the initial structure and to reach a steady state. The applied shear rate was chosen to be large enough to break the filler network, but not too large in order to avoid any expulsion of the nanocomposite which could happen at shear rates larger than a few s^{-1} . The strain applied to the sample is much larger than what would be necessary to reach the steady state (30 strain units, for example, in Lertwimolnum *et al.* (2007)). However the application of a larger strain has no effect since the steady state is reached. Then, the same shear rate was applied again, during the same time but in the reverse direction. This subsequent shear was essentially performed for experimental reasons. Indeed, the rotating plateau position must be accurately reinitialized in order to switch from the permanent shear mode to the oscillatory one. These conditions were selected as leading to similar structures whatever the nanocomposite initial state was. This type of protocol, but with different values of shear rate and time, is often used to obtain a reproducible initial state for all the samples [Lertwimolnum *et al.* (2007), Kim and

Macosko (2009)]. The rheological measurements were carried out in the linear domain, determined by monitoring storage modulus in dynamic strain sweep experiments at low frequency (0.1 rad/s). Linear melt state viscoelastic behaviour was investigated using a decreasing frequency sweep, from 100 to 0.03 rad/s. The decreasing frequency sweep was preferred to the increasing one in order to limit some artefacts when starting from the lower frequency. Indeed the structure evolves with time and this evolution is faster at short times. This means that the structure evolves during the time necessary to measure the lower frequency. For this reason, the frequency lower value was fixed at 0.03 rad/s in order to limit this effect. In some cases, annealing phases were included into the experimental protocol: the sample was then let at rest in the rheometer during a certain time at a fixed temperature.

III. RESULTS AND DISCUSSION

A. X-ray diffraction

Figure 1 shows the WAXD pattern of the OMMT (Dellite[®] 67G) and that of nanocomposites. As it can be seen, the organoclay exhibits three characteristic peaks at 2θ between 2 and 8°. The interlayer spacings associated to those peaks and given by Bragg's equation are indicated in the figure. It should be noted that the WAXD peaks of the matrix do not appear in this angular range. When the organoclay is mixed with PP containing a certain amount of compatibilizer, polymer chains become able to penetrate the layer galleries, giving rise to an increase of the interlayer distance, which is reflected on the WAXD patterns by a shift of the peaks to lower angles. In the present case, interlayer spacing increases from 3.37 nm for the OMMT to 3.70 nm for nanocomposites A and C and 3.87 nm for nanocomposite B. The interlayer distance appears to be function of the PP-g-MA/OMMT ratio: the two nanocomposites with the same PP-g-MA/OMMT ratio present the same intercalation distance, when the nanocomposite B, with the higher PP-g-MA/OMMT ratio, results in a more intercalated structure. As the d_{001} peak is clearly visible on the XRD pattern, we may assume that the nanocomposites are only partially exfoliated.

B. Morphological characterization

The large amount of OMMT in the masterbatches (20 wt%) leads to the presence of large agglomerates, of average diameter in the range 22-25 μm (Figures 2a and 2b). Besides these agglomerates, TEM observations show a certain level of exfoliation and a high concentration

of platelets and tactoids (Figures 2c and 2d). As expected, exfoliation seems to be more important for the sample with the higher PP-g-MA content.

After dilution, the distance between tactoids and/or exfoliated platelets tends to increase, as seen in Figure 3. Observations at a higher magnification, not presented here, show that the average number of platelets per tactoid decreases with the PP-g-MA/OMMT ratio, from 7 to 2, respectively, for nanocomposites A and B. This is also depicted via the variation of the specific density of particles for the two nanocomposites: from 6 to 12 particles. μm^{-2} for nanocomposites A and B, respectively. At the same OMMT content, nanocomposite B with a higher PP-g-MA/OMMT ratio presents a better exfoliation level than nanocomposite A. The organoclay concentration at a fixed PP-g-MA/OMMT ratio does not play a significant role in the conditions we tested as nanocomposites B and C are characterized by tactoids of a few platelets. Apparent particle lengths comprised between 90 and 400 nm are observed for the three nanocomposites samples (A, B and C), which is shorter than the one observed in the masterbatches (see Figures 2c and 2d). This indicates a possible breakage of the platelets during the mixing process.

C. Time-evolution of the rheological behaviour

Figure 4 presents the variations of the storage modulus G' associated to the neat matrix (PP/PP-g-MA) and to the nanocomposite A (85/10/5), after different annealing times (20 to 300 min). As mentioned above, before each annealing, all samples were sheared at a constant shear rate of 1 s^{-1} according to the protocol previously described to obtain a reproducible initial state. It can clearly be seen in Figure 4 that the nanocomposite samples exhibit a pronounced non-terminal behaviour, characterized by an elastic low frequency plateau, indicating interactions between the nanofillers (exfoliated platelets and tactoids). However, this plateau increases with annealing time. It means that the 3D network existing in the system is not stable and evolves with time. When moving to the high frequency domain, the contribution of the matrix polymer chains becomes dominant and, therefore, the curves for different annealing times superimpose perfectly. According to these observations, it is now interesting to study in more details the time evolution of the rheological behaviour of the nanostructured material for different frequencies.

D. Kinetics of the time-evolution of the nanostructure

In a first step, we focus on nanocomposite A. During the pre-shear at 1 s^{-1} , the existing nanostructure resulting from the sample preparation and loading is destroyed, and the platelets and tactoids are oriented in the flow direction (Figure 5). The increase of moduli during annealing time is thus attributed to the build-up of a new nanostructure, reforming after the loss of the previous orientation. In order to evaluate the build-up kinetics of this nanostructure, experiments were performed on the nanocomposite samples at different frequencies and different temperatures, using the scenario drawn in Figure 6. It consists in loading the sample at a given temperature T (180, 200 or 220°C), then applying flow and flow reversal shear at 1 s^{-1} , each during 155 s, and then measuring for a long period of time (up to 20 h) the loss and storage moduli in frequency sweeps (in the linear domain), between 100 and 0.03 rad/s (with 4 points per decade). Each frequency sweep taking around 18 min, we could then have the time evolution associated to these frequencies every 18 min. Total measuring time was around 70 000 s (around 20 h), leading to 65 frequency sweeps. The thermal stability of the matrix was obviously checked before the experiments.

This experimental protocol enables to obtain, for each temperature, the variations of storage and loss moduli versus frequency for different ageing times, as presented in Figure 7. We observe the progressive development of the low frequency plateau on G' , whereas a weaker effect can be seen on G'' . The perfect superposition of the data at high frequency proves the absence of degradation, even at very long time. From these data, we can extract the time evolution of G' for several frequencies, as presented in Figure 8 in double logarithmic scale. At high frequency, G' is stable as it reflects the behaviour of the polymer matrix. But, as soon as the frequency decreases, the time-evolution of G' is more and more visible. Moreover, we can clearly see that this evolution follows a two-step process: above a critical time t_{crit} , around 35 000 s, the kinetics is largely accelerated.

Such changes of G' with time have been shown by Ren *et al.* (2003) who found for PS/OMMT nanocomposites a power law evolution ($G' \propto t^\beta$), with an experimental exponent β between 0.1 and 0.25. Similar observations were made by Kim and Macosko (2009) on graphene/polycarbonate nanocomposites, with β values between 0.3 and 1.4. To our knowledge, only Treece and Oberhausen (2007a,b) and Kim and Macosko (2009) showed a two-step process. Treece and Oberhausen found a time-evolution with two slopes (β_1 and β_2), similar to the ones shown in Fig. 8. Depending on the amount of nanoclay and the preparation procedure, β_1 values were between 0.02 and 0.17, and β_2 between 0.26 and 1.17. In our case,

it can be seen in Figure 9 that β values strongly depend on the frequency used for the experiments. However, β_2 is always higher than β_1 , and both values are all the more high as the frequency is low. According to Treece and Oberhausen (2007a,b), we assume that the first kinetics is related to the disorientation of tactoids and platelets, and the second one to the aggregation of these entities in a 3D network, through van der Waals attractive forces (Fig. 5). As shown in Fig. 9, the description of the kinetics using the slope of G' is inaccurate, as it depends on the frequency. It is the same problem when the slope of the complex viscosity η^* is used to quantify the level of exfoliation [Wagener and Reisinger (2003)]. Moreover, this parameter has no physical meaning. To overcome these problems, we suggested [Lertwimolnun and Vergnes (2005), Vergnes (2011)] to fit the complex viscosity curve by a Carreau-Yasuda law with a yield stress:

$$\eta^*(\omega) = \frac{\sigma_0}{\omega} + \eta_0 [1 + (\lambda\omega)^a]^{(m-1)/a} \quad (1)$$

where σ_0 is the melt yield stress, η_0 the zero-shear viscosity, λ the time constant, a the Yasuda parameter and m the dimensionless power law index. This model contains five parameters that are adjusted for obtaining the best fit with the experimental data (Microsoft Solver in Excel is used for this purpose). It has been shown that the value of the melt yield stress σ_0 , which is unique and unambiguously defined for a fixed viscosity curve, is a good indicator of the exfoliation level (or more generally of the interactions between the nanofillers) [Lertwimolnun and Vergnes (2005, 2006, 2007)]. By treating the data of Fig. 7 with the formalism of Eq. (1) and extracting the values of the melt yield stress, we can now plot its evolution with time, as shown in Figure 10. As for the storage modulus, we observe a kinetics in two steps. The first one (platelets disorientation) can be described by a square root:

$$\sigma_0 = C_1 \sqrt{t} \quad \text{when } t < t_{crit} \quad (2)$$

and the second one (network aggregation) by a linear expression:

$$\sigma_0 = C_1 \sqrt{t_{crit}} + C_2 (t - t_{crit}) \quad \text{when } t > t_{crit} \quad (3)$$

where C_1 and C_2 are constants.

In order to confirm these results, experiments were repeated using sample B. As said before, this 5 wt% OMMT nanocomposite presents a higher level of exfoliation compared to sample A (see Fig. 3) thanks to a higher PP-g-MA content. Figure 11 shows the time evolution of melt yield stress for these two nanocomposites. The same behaviour is observed, with the same kind of evolution, but with a faster progression for sample B: the critical time is shorter

and the melt yield stress is always higher than for sample A. We may assume that it is a consequence of a higher exfoliation level, inducing more interactions between individualized platelets.

Nanocomposite C has the same PP-g-MA/OMMT ratio as sample B, but a higher OMMT content (7 wt.%). Figure 12 shows once again the same time evolution, with higher critical time and melt yield stress values, probably due to the more concentrated structure. It seems thus that the behaviour described by equations (2) and (3) is common to these nanocomposite systems, with a first kinetics related to the loss of orientation of the platelets or tactoids, and a second one related to the formation of a 3D network. It is important to notice that, even at very long times, the structure of the nanocomposites does not seem to stabilize. Treece and Oberhausen (2007a,b) suggested therefore to consider these materials as belonging to the class of soft colloidal glasses.

In order to go further in the understanding of this time evolution, we investigated the effect of temperature on the kinetics. Experiments were conducted on the nanocomposite A at three different temperatures (180, 200 and 220°C). As it can be seen in Figure 13, the general tendency of evolution given by Eqs. (2) and (3) remains valid, but the kinetics is modified by the temperature: when the temperature increases, the critical time t_{crit} is shorter and both kinetics are more rapid, C_1 and C_2 being functions of the temperature.

The different values of parameters C_1 , C_2 and t_{crit} are reported in Table 2. If the first kinetics is assumed to be due to the disorientation of the platelets by Brownian motion, t_{crit} should be related to the rotary diffusion coefficient D_{r0} [Larson (1999), Ren *et al.* (2003)]:

$$D_{r0} = \frac{3k_B T}{4\eta_0(T) d^3} \quad (4)$$

where k_B is the Boltzmann constant, T the absolute temperature and d the diameter of the tactoid.

Table 2. Parameters of Eqs. (2) and (3) for the various nanocomposites

| Sample | Temperature (°C) | C_1 (Pa.s ^{-0.5}) | C_2 (Pa.s ⁻¹) | t_{crit} (s) |
|--------|---------------------|----------------------------------|--------------------------------|-------------------|
| A | 180 | 1.3 | 0.0037 | 50 300 |
| A | 200 | 3.9 | 0.025 | 38 500 |

| | | | | |
|---|-----|-----|-------|--------|
| A | 220 | 4.5 | 0.040 | 20 300 |
| B | 200 | 6 | 0.070 | 12 800 |
| C | 200 | 18 | 0.085 | 22 400 |

Figure 14 compares the values of t_{crit} and the time related to the rotary diffusion ($1/D_{r0}$) for the three temperatures. The rotary diffusion coefficient is calculated using the Newtonian viscosity of the PP/PP-g-MA matrix and for a range of tactoid diameters, between 100 and 500 nm. It can be seen in Fig. 14 that the two parameters vary in the same way with the temperature. However the time related to the rotary diffusion is much shorter than the time corresponding to the end of the first step of the structure evolution. This was also noted by Mobuchon *et al.* (2007). If the tactoid diameter d is evaluated from t_{crit} , we obtain $d \approx 1.35 \mu\text{m}$, which is much higher than the values of 90-400 nm estimated from TEM observations. For these dimensions, the rotary diffusion time would be around 1000 s, which is much shorter than the times reported here. Consequently, even though Brownian motion of the platelets and tactoids may play a role in the first part of the kinetics, other mechanisms are also to be considered.

E. Validity of the time-temperature superposition principle

The rheological properties of the PP/PP-g-MA/organoclay nanocomposites shown before prove their ability to form a 3D network. Moreover, the continuous evolution of this nanostructure shows that it never reaches a thermodynamically stable state in the conditions we tested. Therefore, the validity of the time-temperature superposition principle can be questioned. In a first time, TTS principle was checked on nanocomposite A using an isothermal frequency sweep, after shearing each sample in flow and flow reversal during 155 s and allowing it to relax for the same period of 20 min. The results obtained are shown on Figure 15a. At high frequency, we observe a classical decrease of modulus with temperature. But, at low frequency, the plateau is all the more high as the temperature is high. Consequently, by shifting the curves along the frequency axis to apply TTS principle, we observe in Figure 15b a complete failure of this principle. At high frequency, the curves superimpose perfectly, as the polymer chains govern the rheological properties, but, at low frequency, the curves diverge. Such behaviour was expectable as it is typical for samples with properties changing during the experiments. We have seen before (Fig. 13) that, for a fixed

annealing time of 20 min, the kinetics of structure formation were different according to the temperature, leading to materials with different nanostructures. If we want to correctly apply TTS principle, we have to select, for each temperature, an annealing time providing the same nanostructure, i.e. the same yield stress (Fig. 13). As an example, let us consider that the reference state is the one obtained after 38 520 s at 180°C (horizontal dotted line in Fig. 13). The same yield stress (252 Pa) is obtained after 3360 s at 200°C and 2160 s at 220°C. The data (G' and G'') corresponding to these different times are presented in Fig. 16. If we now apply the TTS principle to these data, using only the frequency shift factor a_T , it is possible to obtain a perfect master curve for G' and G'' (Figure 17).

This time-temperature equivalence indicates that, for a same nanostructure, all the processes, including the non-terminal behaviour related to the organoclay and also the high frequency relaxations, change with temperature in the same manner. Therefore, increasing temperature only accelerates structure build-up and we can conclude that there are equivalences or similarities between the nanostructures characterized by the same melt yield stress. Subsequent time-temperature superposition based on another value of yield stress (367 Pa) was also successfully tested. The shift factors a_T used to construct the mastercurves associated to the neat matrix and to the nanocomposites are nearly identical (see Table 3), leading to very close values of activation energy (40 kJ/mol, see Table 4).

This result implies that the temperature dependence being probed is that of the polymer. Since the silicate layers do not have a temperature dependant relaxation, the only relaxation process dependent on temperature is that of the polymer segments. Such a result, implying that the addition of inorganic clays significantly affects the magnitude of G' and G'' but not the characteristics of the time-temperature superposition, has been previously observed for nanostructured materials with different kinds of matrices and nanofillers [Krishnamoorti and Giannelis (1997); Ren *et al.* (2000); Solomon *et al.* (2001)].

Table 3. Shift factor a_T for the matrix and the nanocomposite A for two values of the melt yield stress

| Temperature (°C) | a_T matrix | a_T | a_T |
|---------------------|-----------------|--------------------------------------|--------------------------------------|
| | | nanocomposite $\sigma_0 = 252$ Pa | nanocomposite $\sigma_0 = 367$ Pa |
| 180 | 1 | 1 | 1 |
| 200 | 0,60 | 0,68 | 0,68 |
| 220 | 0,39 | 0,42 | 0,44 |

Table 4. Activation energy for the matrix and the nanocomposite A for two values of the melt yield stress

| Sample | Matrix | Nanocomposite | Nanocomposite |
|-------------|------------|---------------------|---------------------|
| | | $\sigma_0 = 252$ Pa | $\sigma_0 = 367$ Pa |
| Ea (kJ/mol) | 44 ± 5 | 41 ± 5 | 38 ± 5 |

Since temperature only accelerates the formation of the 3D network, it should be possible to get mastercurves by annealing the samples at the highest temperature (220°C in our case) in order to induce fast morphological changes of the nanostructure, before performing measurements at the selected temperature. This protocol has been successfully used by Reichert *et al.* (2001) to generate a mastercurve associated to PP/organoclay nanocomposites with unstable microstructure. The experimental protocol is as follows: after pre-shear in forwards and backwards directions, each for 155 s at 1 s^{-1} , the sample is let at rest at 220°C for 40 min. Then, the temperature is decreased, down to the selected temperature (180 or 200°C) in approximately 13 min, and the frequency sweep is started, from 100 to 0.01 rad/s. It is to be noted that, for these experiments, we used parallel plate geometry, and the thermal dilatation of the plates has been taken into account in order to avoid artefacts associated with lack of material in the gap. Figure 18 evidences that, using a thermal treatment at the highest temperature, the TTS principle holds on the whole tested frequency range. Although less perfect than when probing different annealing times (Fig. 17), the superposition is really good

relatively to the one obtained with the classical protocol as shown in Figure 15. It confirms the conclusion that the rheological behaviour of the nanocomposite remains governed by the same physical phenomena, which are only accelerated with temperature increase.

IV. CONCLUSION

We have investigated the melt linear viscoelastic properties of layered silicate based polymer nanocomposites under oscillatory shear. We have studied the evolution of the storage modulus G' at different frequencies as it reflects the evolution of the system at multiscale. At high frequency, where the polymer chains govern the behaviour of the material, G' is almost stable. On the contrary, at low frequency, G' presents a monotonic increase with time, associated to the continuous build-up of a structure. The melt yield stress (obtained by fitting the viscosity curve with a Carreau-Yasuda model with a yield stress) was used to follow the nanostructure evolution and avoid any frequency dependence of the parameter. We have quantified the kinetics of this structure build-up and shown that it was a two-step process. The first one is attributed to platelets disorientation and the second one, faster, to the aggregation of platelets and tactoids in a 3D network. This structure evolution was observed for different formulations of nanocomposites based on PP, PP-g-MA and organoclay whose structure is partially exfoliated and intercalated and where the nanoclays form a more or less soft network. This feature should be valid for other nanocomposites characterized by a similar structure. It varies drastically with temperature. Consequently, it violates the time-temperature superposition principle. However, we proved that the time-temperature equivalence exists if we anneal samples for different times, depending on temperature, in order to obtain similar nanostructures, quantified by a same melt yield stress. This time-temperature equivalence evidences that, for a fixed nanostructure, the only relaxation process involved is that of the polymer chains, and that the behaviour of the nanocomposite is governed by the same physical phenomena for the whole temperature range investigated here. Finally, as temperature does not induce any change through chemical interactions within the system, a thermal treatment applied to the nanocomposite at a high temperature could be a solution to obtain time-temperature equivalence.

Acknowledgement

Authors thank Julien Ville, Rudy Valette and Patrick Navard from CEMEF for fruitful discussions and Aleksey Drosdov from Denmark Technical University (DTU, Lyngby,

Denmark) for gently providing the masterbatch. Financial support by the European Commission through project Nanotough-213436 is gratefully acknowledged. The authors are also grateful to the referees for interesting suggestions allowing to improve the paper.

References

- Alexandre, M. and P. Dubois, "Polymer-layered silicate nanocomposites: preparation, properties and use of a new class of materials", *Mater. Sci. Eng.*, **28**, 1-63 (2000).
- Cassagnau, Ph. "Melt rheology of organoclay and fumed silica nanocomposites," *Polymer*, **49**, 2183-2196 (2008).
- Drosdov A. D., E.A. Jensen and J. de C., Christiansen, "Non-linear time-dependent response of polypropylene/nanoclay melts: Experiments and modelling," *Comp. Mat. Sci.*, **47**, 807-816 (2010).
- Elasmi, H., M. Grmela, and M. Bousmina, "Linear and nonlinear rheology of polymer/layered silicate nanocomposites," *J. Rheol.*, **54**, 539-562 (2010).
- Gilman, J.W., "Flammability and thermal stability studies of polymer-layered silicate (clay) nanocomposites," *Appl. Clay Sci.*, **15**, 31-49 (1999).
- Kim, H., C. W. Macosko, "Processing-property relationships of polycarbonate/graphene composites", *Polymer*, **50**, 3797-3809 (2009).
- Krishnamoorti, R., R.A. Vaia and E.P. Giannelis, "Structure and dynamics of polymer-layered silicate nanocomposites", *Chem. Mater.*, **8**, 1728-1734 (1996).
- Krishnamoorti R., and E. P. Giannelis, "Rheology of end-tethered layered silicate nanocomposites," *Macromol.*, **30**, 4097-4102 (1997).
- Larson, R.G., "The Structure and Rheology of Complex Fluids", Oxford University Press: New York, 1999.
- Lertwimolnun, W., and B. Vergnes, "Influence of compatibilizer and processing conditions on the dispersion of nanoclay in a polypropylene matrix," *Polymer*, **46**, 3462-3471(2005).

- Lertwimolnun, W., and B. Vergnes, "Effect of processing conditions on the formation of polypropylene/organoclay nanocomposites in a twin screw extruder," *Polym. Eng. Sci.*, **46**, 314-323 (2006).
- Lertwimolnun, W., B. Vergnes, G. Ausias, and P.J. Carreau, "Stress overshoots of organoclay nanocomposites in transient shear flow", *J. Non-Newt. Fluid Mech.*, **141**, 167-179 (2007).
- Lertwimolnun, W., and B. Vergnes, "Influence of screw profile and extrusion conditions on the microstructure of polypropylene/organoclay nanocomposites", *Polym. Eng. Sci.*, **47**, 2100-2109 (2007).
- Loiseau, A., and J.F. Tassin, "Model nanocomposites based on laponite and poly(ethylene oxide): preparation and rheology", *Macromol.*, **39**, 9185-9191 (2006).
- Messersmith P.B., and E.P. Giannelis, "Synthesis and barrier properties of poly(ϵ -caprolactone)-layered silicate nanocomposites," *J. Polym. Sci., Part A: Polym. Chem.*, **33** 1047-1057 (1995).
- Mobuchon, C., P.J. Carreau and M.-C. Heuzey, "Effect of flow history on the structure of a non-polar polymer/clay nanocomposite model system", *Rheol. Acta*, **46**, 1045-1056 (2007).
- Mobuchon, C., P.J. Carreau, and M.C. Heuzey, "Structural analysis of non-aqueous layered silicate suspensions subjected to shear flow," *J. Rheol.*, **53**, 1025-1048 (2009).
- Nazockdast E., H. Nazockdast, and F. Goharpey, "Linear and non-linear melt-state viscoelastic properties of polypropylene/organoclay nanocomposites," *Polym. Eng. Sci.*, **48**, 1240-1239 (2008).
- Palvidou, S., and C.D. Papaspyrides, "A review on polymer-layered silicate nanocomposites," *Prog. Polym. Sci.*, **33**, 1119-1198 (2008).

- Paul, D.R., and L.M. Robeson, "Polymer nanotechnology: nanocomposites", *Polymer*, **49**, 3187-3204 (2008).
- Reichert, P., B. Hoffmann, T. Bock, R. Thomann, R. Mullhaupt, and C. Friedrich, "Morphological stability of Poly(propylene) nanocomposites," *Macromol. Rapid Commun.*, **22**, 519-523 (2001).
- Ren, J., A. S. Silva, and R. Krishnamoorti, "Linear viscoelasticity of disordered polystyrene-polyisoprene block copolymer based layered-silicate nanocomposites," *Macromol.*, **33**, 3739-3746 (2000).
- Ren, J., B.F. Casanueva, C.A. Mitchell, and R. Krishnamoorti, "Disorientation kinetics of aligned polymer layered silicate nanocomposites", *Macromol.*, **36**, 4188-4194 (2003).
- Solomon, M. J., A. S. Almusallam, K. F. Seefeldt, A. Somwangthanaroj and P. Varadan, "Rheology of Polypropylene/clay hybrid materials," *Macromol.*, **34**, 1864–1872 (2001).
- Treece, M.A., and P. Oberhauser, "Soft glassy dynamics in polypropylene-clay nanocomposites", *Macromol.*, **40**, 571-582 (2007a).
- Treece, M.A., and P. Oberhauser, "Ubiquity of soft glassy dynamics in polypropylene-clay nanocomposites", *Polymer*, **48**, 1083-1095 (2007b).
- Vergnes, B., "The use of apparent yield stress to characterize exfoliation in polymer nanocomposites", *Int. Polym. Proc.*, **26**, 229-232 (2011)
- Vermant, J., S. Ceccia, M. K. Dolgovskij, P. L. Maffetone, and C. W. Macosko, "Quantifying dispersion of layered nanocomposites via melt rheology," *J. Rheol.*, **51**, 429-450 (2007).
- Wagener, R., and T.J.G. Reisinger, "A rheological method to compare the degree of exfoliation of nano-composites", *Polymer*, **44**, 7513-7518 (2003).

Xu, R., E. Manias, A.J. Snyder and J. Runt, “New biomedical poly(urethane urea)-layered silicate nanocomposites,” *Macromol.*, **34**, 337–339 (2001).

Zhao, J., A.B. Morgan, and J.D. Harris, “Rheological characterization of polystyrene-clay nanocomposites to compare the degree of exfoliation and dispersion”, *Polymer*, **46**, 8641-8660 (2005).

Figure captions

Figure 1. X-ray diffraction patterns of the initial organoclay (Dellite 67G) and the nanocomposites. Interlayer distances are indicated above the peaks.

Figure 2. Microscopy observations of the masterbatches.

(a) SEM, 80/20 PP-g-MA/OMMT; (b) SEM 40/40/20 PP/PP-g-MA/OMMT;

(c) TEM, 80/20 PP-g-MA/OMMT; (d) TEM, 40/40/20 PP/PP-g-MA/OMMT.

Figure 3. TEM observations of the nanocomposites :

(a) A (85/10/5 PP/PP-g-MA/OMMT); (b) B (75/20/5 PP/PP-g-MA/OMMT);

(c) C (65/28/7 PP/PP-g-MA/OMMT)

Figure 4. Variations of storage modulus G' with frequency at 200°C for the matrix (PP/PP-g-MA, ○) and for the nanocomposite A (85/10/5) annealed at 200°C for 20 min (●), 130 min (□) and 300 min (■).

Figure 5. Schematic description of structure changes during shear flow (from (a) to (c)) and at rest (from (c) to (a)).

Figure 6. Experimental protocol used to probe the evolution of the structure using successive frequency sweeps

Figure 7. Time variations of storage modulus G' (a) and loss modulus G'' (b) of nanocomposite A (85/10/5) at 200°C. The time increases from bottom to top.

Figure 8. Time evolution of storage modulus G' of nanocomposite A (85/10/5) for different frequencies at 200°C. The vertical line indicates the critical time where the kinetics changes.

Figure 9. Variation of the power law exponents of the time evolution of G' with frequency. The insert gives the definition of the exponents.

Figure 10. Time evolution of the melt yield stress σ_0 of nanocomposite A (85/10/5) at 200°C. Symbols are experimental data, full lines are theoretical fits using Eqs. (2) and (3).

Figure 11. Comparison of the time evolution of the melt yield stress σ_0 for nanocomposites A (85/10/5) and B (75/20/5) at 200°C (nanocomposites with the same amount of OMMT but different level of exfoliation). Symbols are experimental data, full lines are theoretical fits using Eqs. (2) and (3).

Figure 12. Comparison of the time evolution of the melt yield stress σ_0 for nanocomposites B (75/20/5) and C (65/28/7) at 200°C (nanocomposites with different amounts of OMMT but the same PP-g-MA/OMMT ratio). Symbols are experimental data, full lines are theoretical fits using Eqs. (2) and (3).

Figure 13. Time evolution of the melt yield stress σ_0 of nanocomposite A (85/10/5) for different temperatures (180°C, 200°C and 220°C). Vertical lines indicate the critical times associated to the change in temporal kinetics for the different temperatures. The horizontal line indicates the times associated to a same yield stress for different temperatures.

Figure 14. Comparison between critical time t_{crit} and rotary diffusion time for different particle diameters as function of temperature (nanocomposite A).

Figure 15. Variations of storage modulus G' with frequency for three temperatures (\square : 220°C \bullet : 200°C \circ : 180°C) at the same annealing time (a) and corresponding curves obtained by TTS (b). The curve obtained at 180°C is taken as reference.

Figure 16. Variations of storage modulus G' (a) and loss modulus G'' (b) with frequency, for three temperatures (\square : 220°C \bullet : 200°C \circ : 180°C) and three annealing times (\square : 2160 s \bullet : 3360 s \circ : 38 520 s) leading to the same yield stress.

Figure 17. Mastercurves of storage modulus G' (a) and loss modulus G'' (b) obtained by TTS of the curves of Fig. 16. Curves obtained at 180°C are taken as reference.

Figure 18. Variations of storage modulus G' for three temperatures (\square : 220°C \bullet : 200°C \circ : 180°C) after annealing at 220°C (a) and corresponding mastercurve obtained by TTS (b). The curve obtained at 180°C is taken as reference.

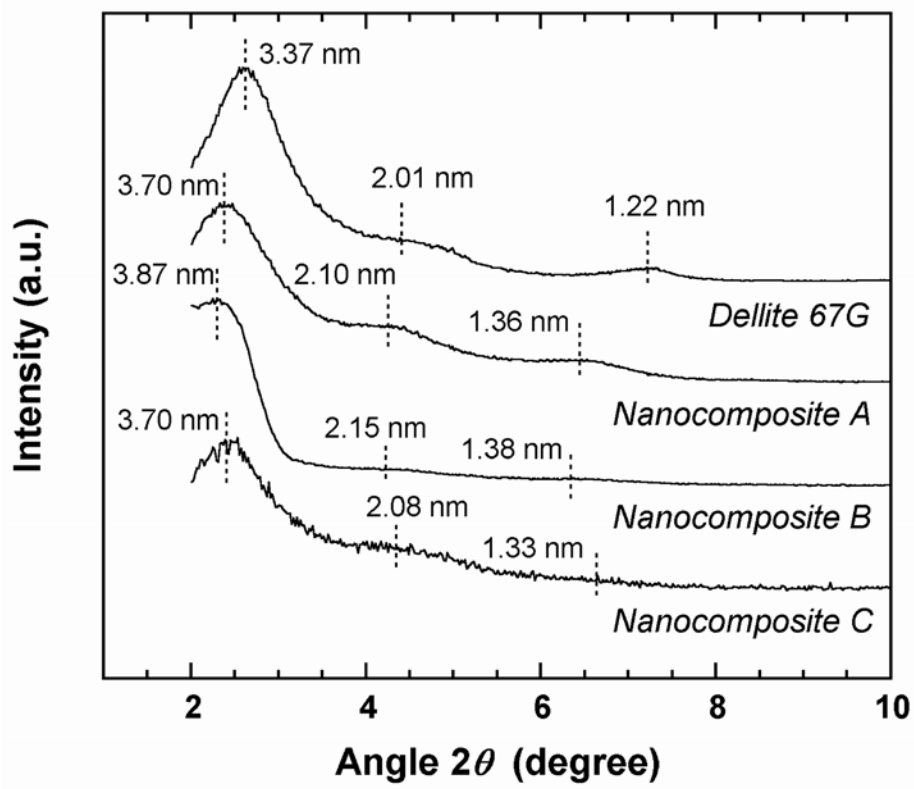


Fig. 1. Zouari et al.

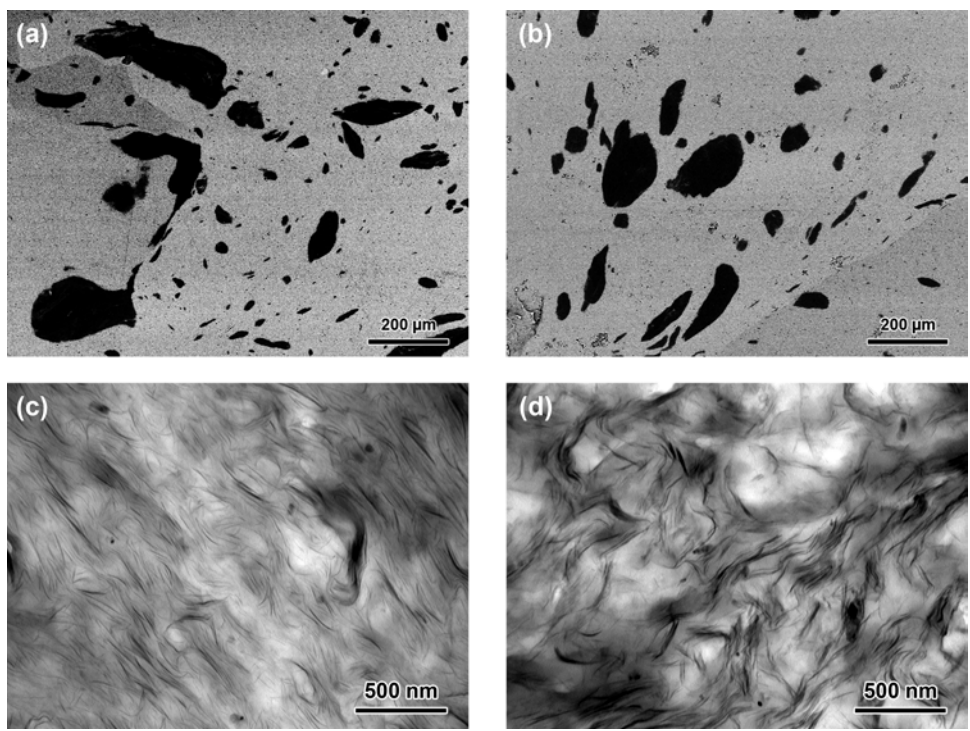


Fig. 2. Zouari et al.

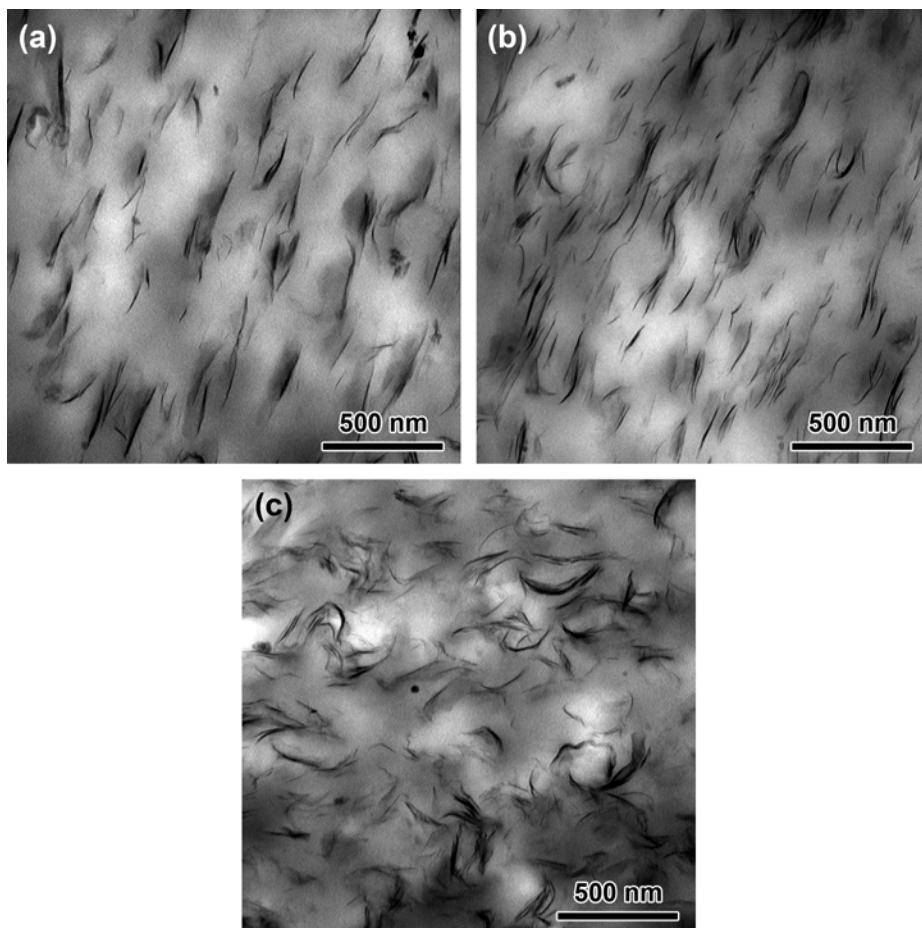


Fig. 3. Zouari et al.

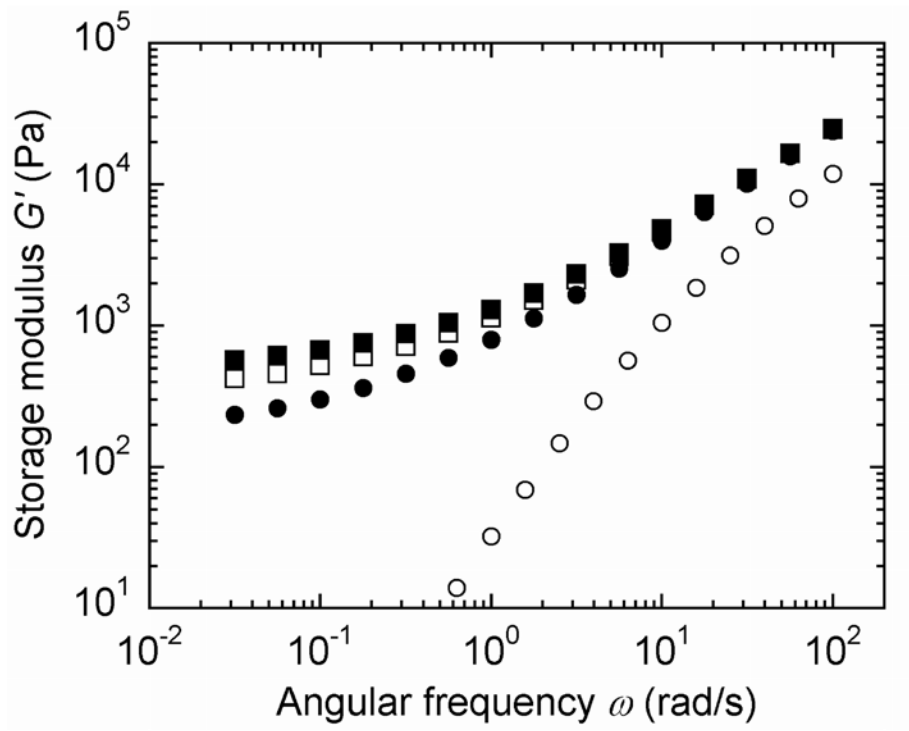


Fig. 4. Zouari et al.

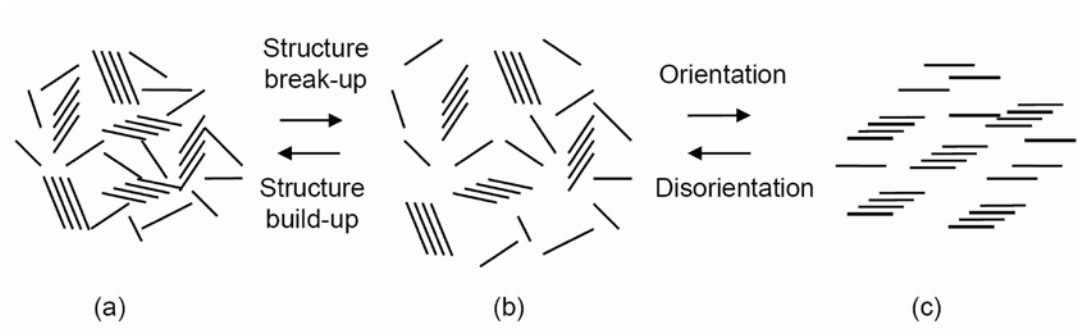


Fig. 5. Zouari et al.

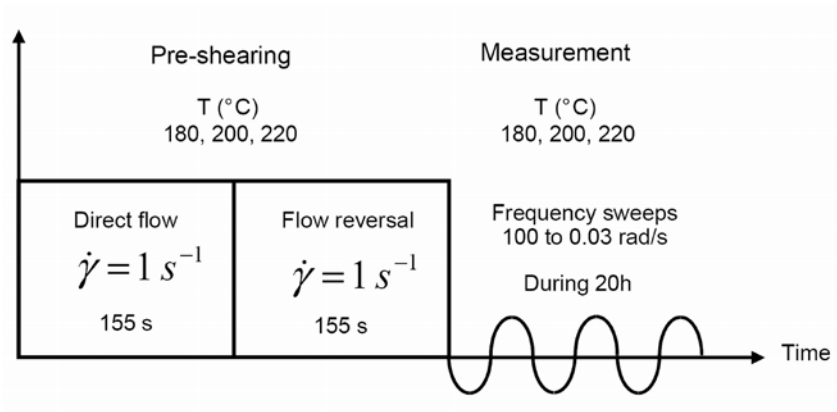


Fig. 6. Zouari et al.

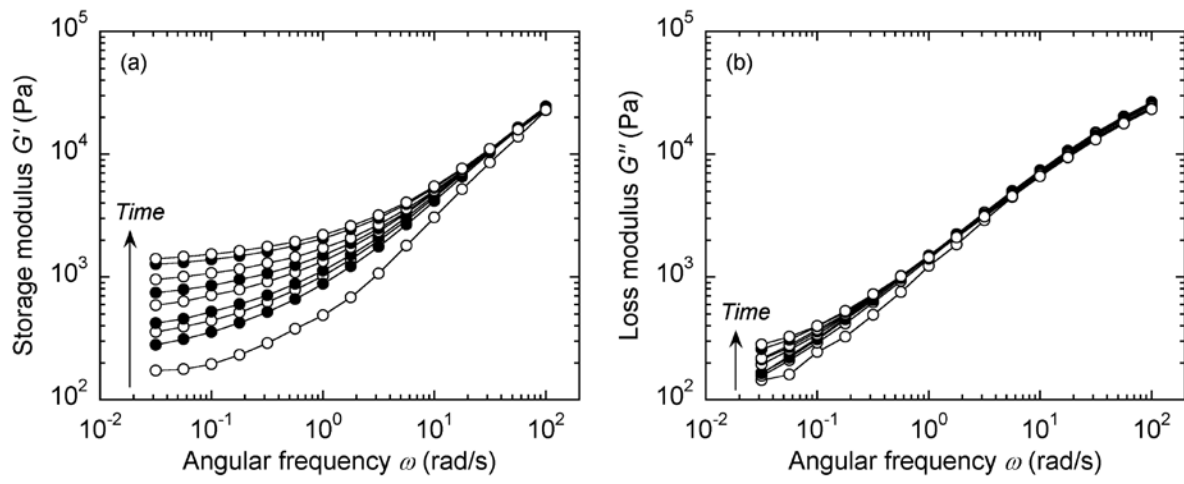


Fig. 7. Zouari et al.

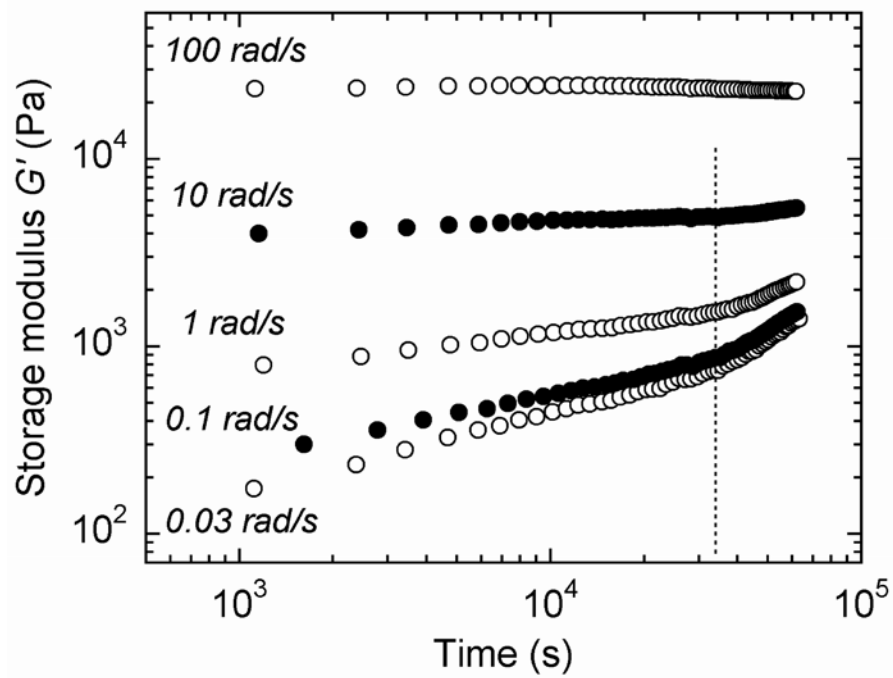


Fig. 8. Zouari et al.

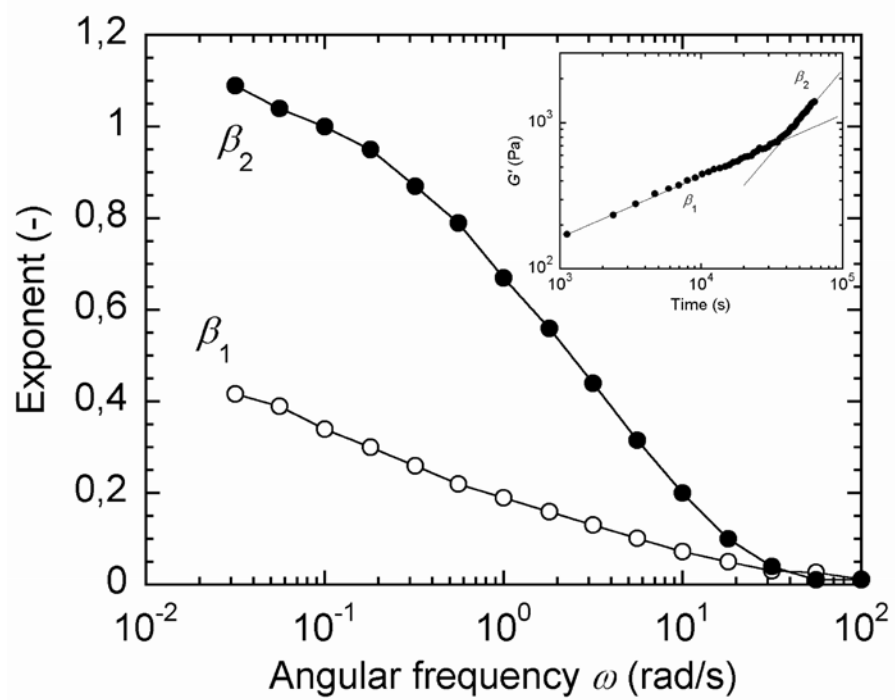


Fig. 9. Zouari et al.

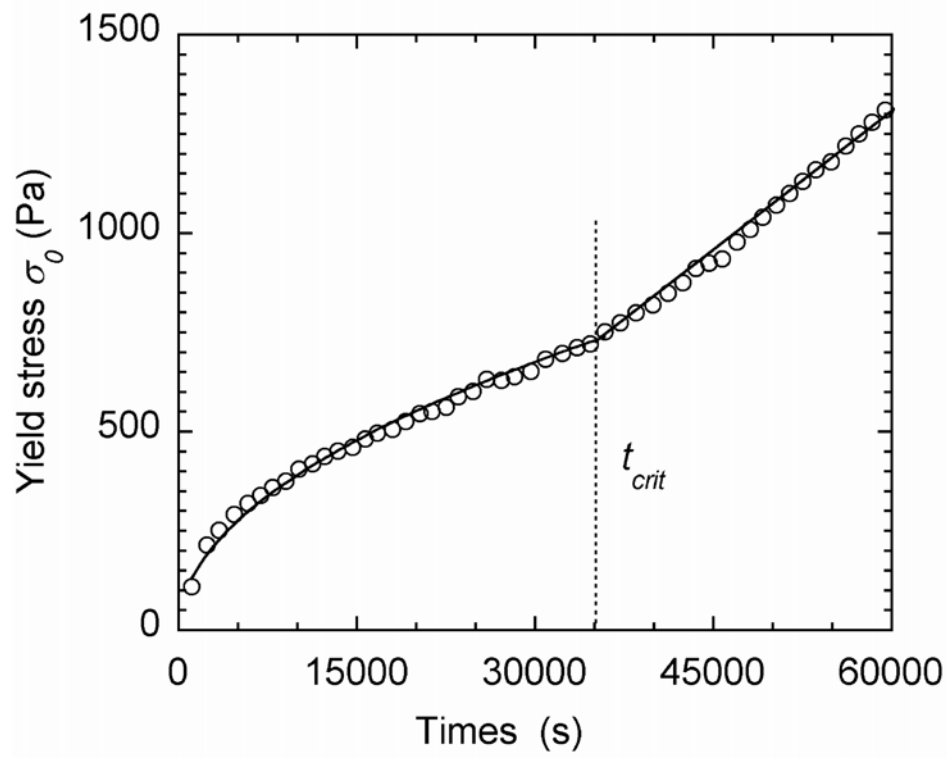


Fig. 10. Zouari et al.

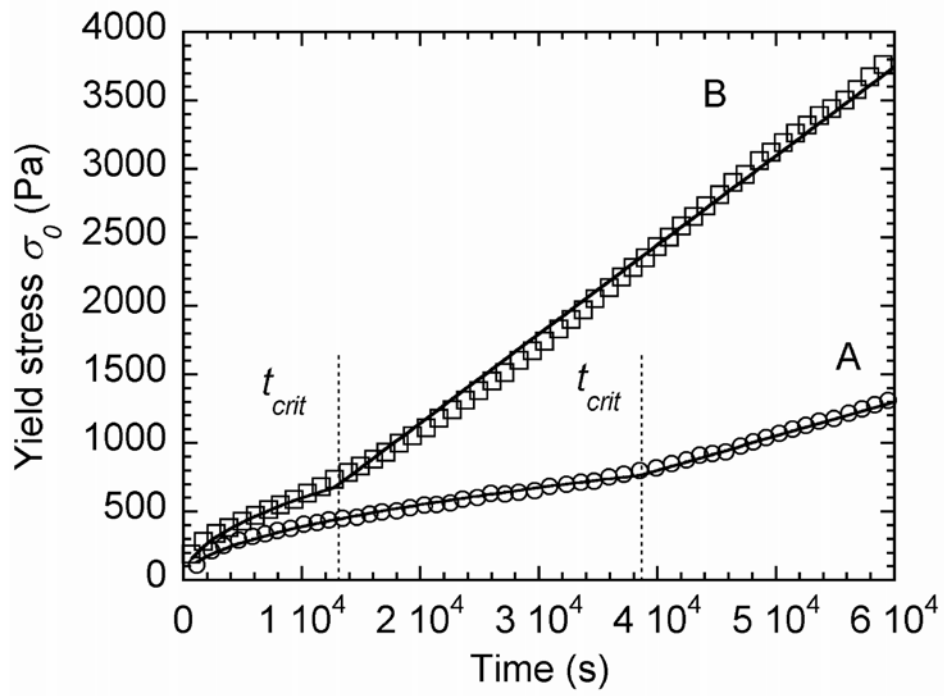


Fig. 11. Zouari et al.

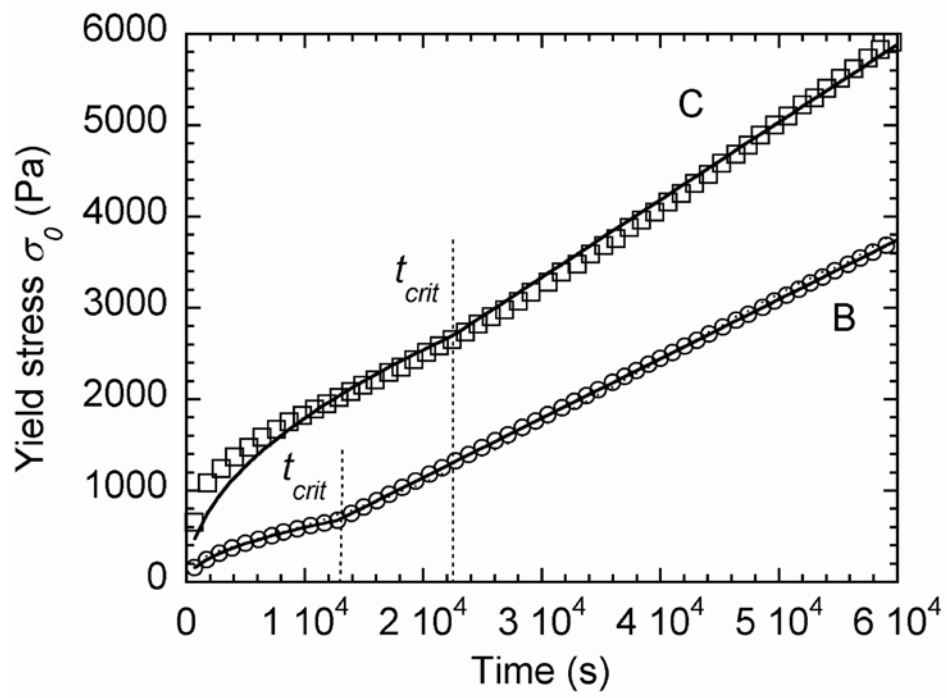


Fig. 12. Zouari et al.

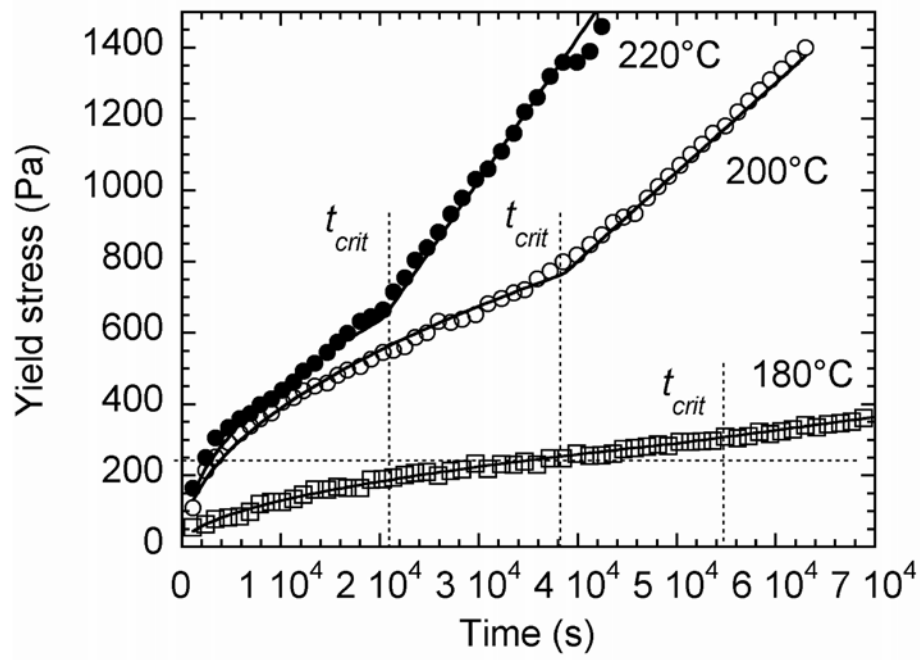


Fig. 13 . Zouari et al.

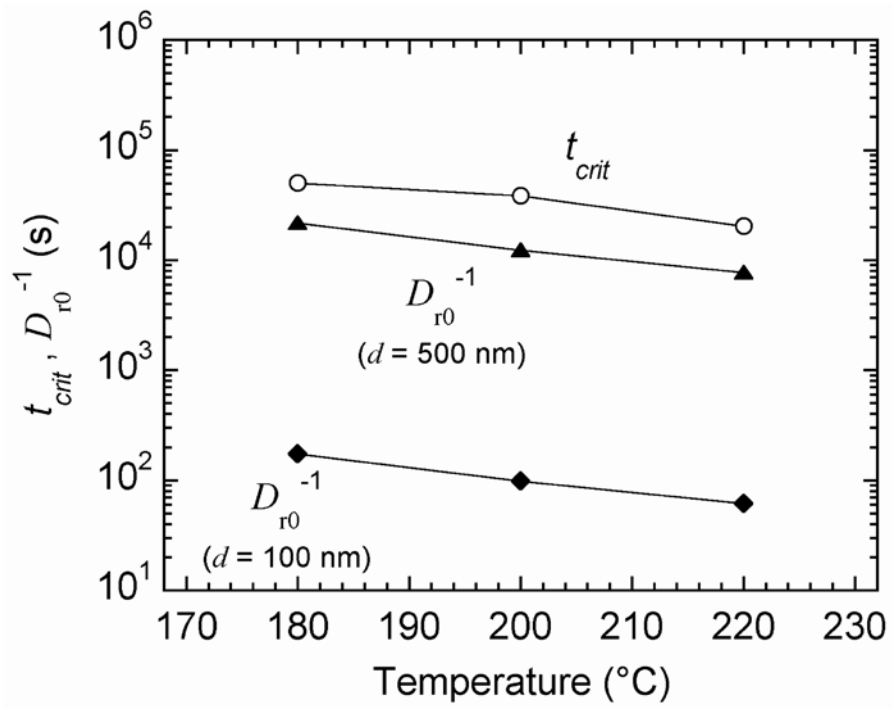


Fig. 14 . Zouari et al.

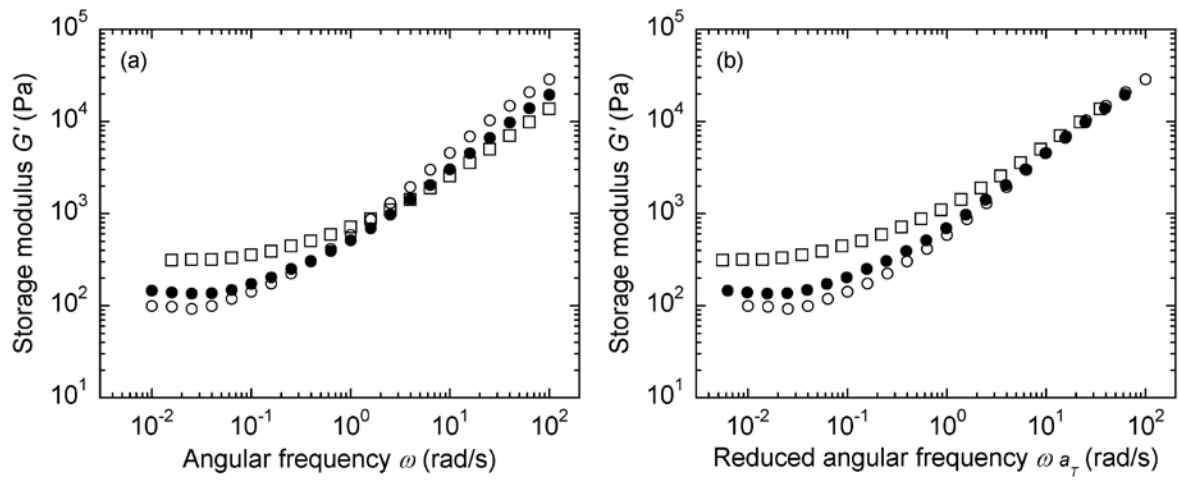


Fig. 15. Zouari et al.

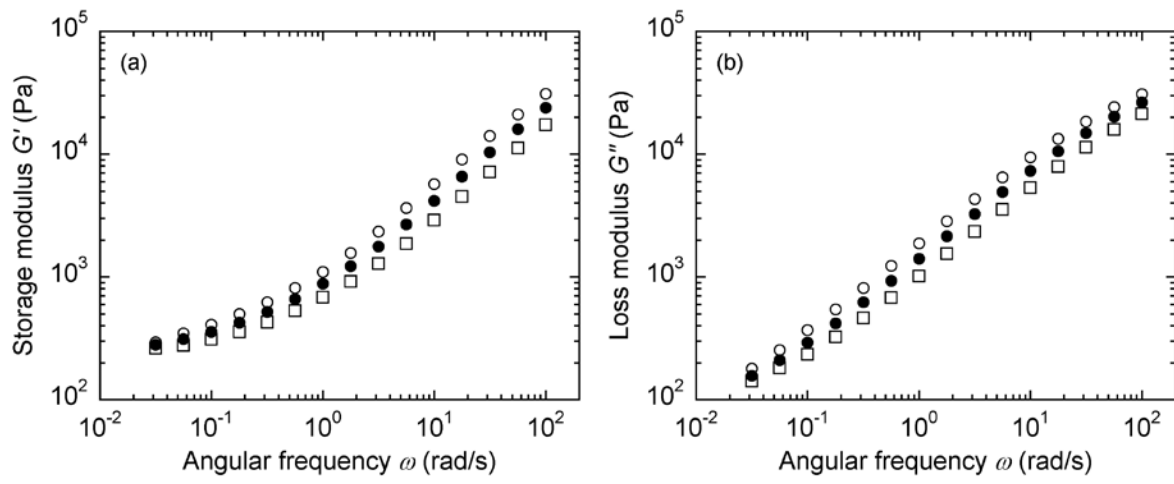


Fig. 16. Zouari et al.

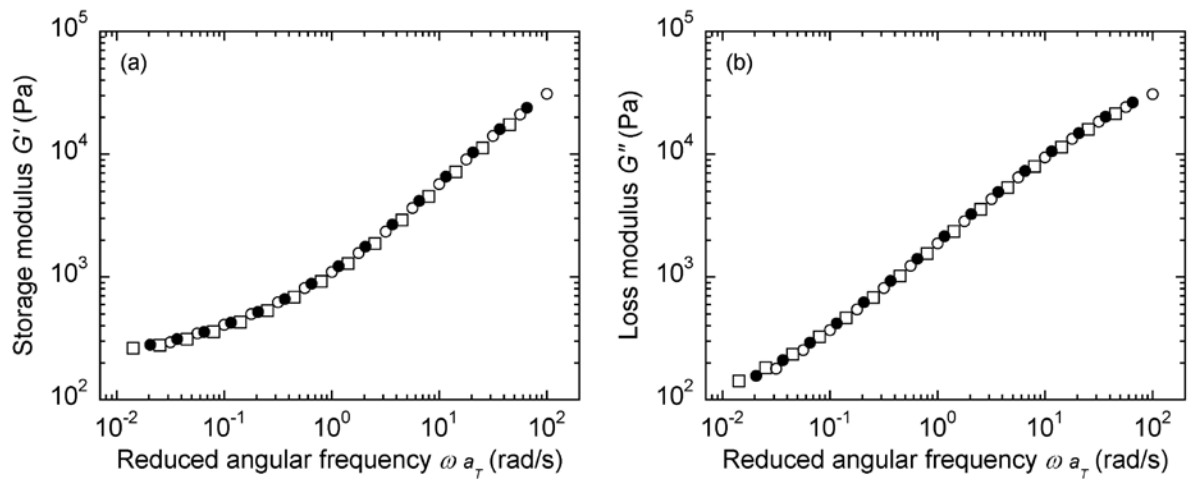


Fig. 17. Zouari et al.

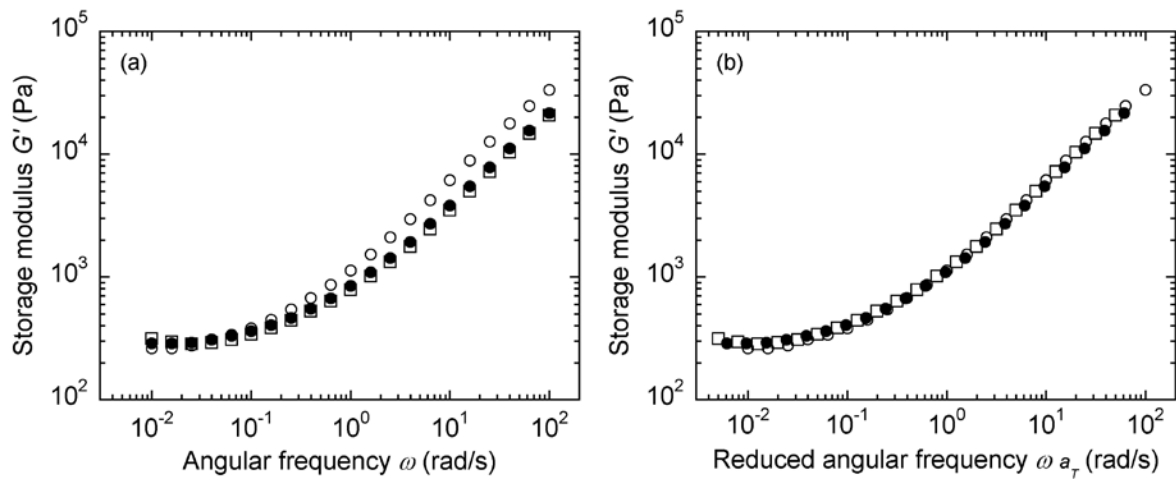


Fig. 18 . Zouari et al.